


Structure, design, and mechanics of a paper spring

Taiju Yoneda,^{*} Daichi Matsumoto, and Hirofumi Wada[†]

Department of Physical Sciences, Ritsumeikan University, Kusatsu, Shiga 525-8577, Japan

 (Received 31 January 2019; published 16 July 2019)

A paper spring is a simple paper craft popular with children. It can be constructed by interfolding and gluing two long strips of paper of equal sizes, with the simplest possible crease patterns. In addition to its curious springy response, this origami-based composite exhibits a twist deformation during its extension. Although its interlocking structure is expected to underly the strong stretch-twist coupling, a detailed understanding of it remains elusive. Here we quantify the kinematics and mechanics of a paper spring during its extensional actuation by combining experimental, numerical, and analytical approaches. We directly link the nonlinear mechanics of a paper spring with its structural design and the sheet elasticity. We show that the unique interlocking provides an enhanced structural rigidity because the thin sheets suffer from geometric frustrations and must locally bend and stretch during extension. This structural design allows for a reversible transformation between the rotatory and linear motions solely by controlling forces and moments applied at the ends of the structure. Such deployment kinematics could provide a unique avenue of the mode conversion for potential applications and will broaden the possibilities of future designs of origami-based springs with tunable functionalities.

DOI: [10.1103/PhysRevE.100.013003](https://doi.org/10.1103/PhysRevE.100.013003)

I. INTRODUCTION

Foldable thin structures are ubiquitous in engineering, arts, architecture, and biology. Among others, origami art defines the formation of complex three-dimensional (3D) geometry from a simple flat sheet via folding with prescribed crease patterns [1–3]. The beauty of origami geometry can be found in a number of biological systems such as plants [4,5] and insect wings [6,7] and is currently exploited in a wide range of applications, including solar sails [8], airbags [9], stent grafts [10], soft robotics, and mechanical metamaterials [11].

Over the last decade, the mechanics of origami has become an active research field in physics. This is in contrast to the classic rigid origami study that concerns the geometry of an idealized rigid-face, zero-thickness origami. The mathematics of rigid origami has established a powerful knowledge base on the design space of possible folding patterns [12]. It fails, however, to provide insight into the stiffness or elasticity of real physical origami made of thin sheets of finite thickness and material properties.

The study of origami mechanics focuses on this aspect. Recent studies have successfully explained emergent resorting forces and moments during folding and unfolding processes in terms of energetic costs in elastic hinges [13]. However, it has also been recognized that the hinge elasticity alone is not sufficient to understand the multistability and snapping dynamics in a class of origami-like foldable structures found in manmade and natural systems [14–17]. For those problems, the bending and twisting of plates is known to be essential, much like in the study of elastic shells [18].

A complete understanding of the geometric mechanics of *elastic* origami is challenging, especially when a crease pattern allows for bistable or multistable morphing pathways. To highlight the role of plate elasticity in the mechanics of foldable structures, here we propose to investigate a specific system—an origami-inspired spring that is known as a paper spring; see Fig. 1. This simple paper craft is made by folding and gluing a pair of long strips of paper of equal sizes [20]. The basic crease pattern of each strip is very simple, an accordion-like parallel fold [21], yet an intriguing mechanical behavior emerges from the coupling of its unique interlocking structure and the sheet elasticity. For instance, the spring overall exhibits an enhanced structural rigidity upon stretching, because the thin sheets suffer from geometric frustrations and must locally bend and stretch, similarly to zipper-coupled

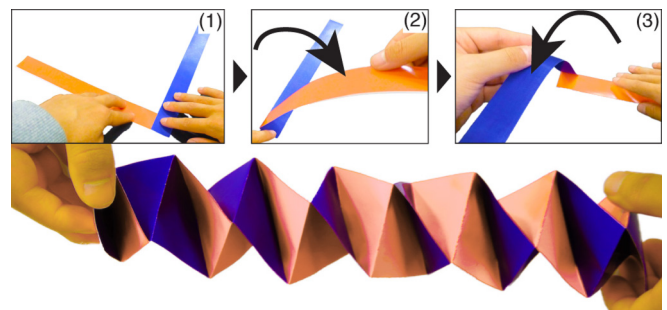


FIG. 1. How to make a paper spring. (1) Begin with two long strips of paper of equal sizes, glue them together such that they form a right angle. (2) Fold the lower strip over the top one, then (3) fold the strip that just came to the lower layer over the one on top. Continue this process (the lower strip always folds over the top one), until the last fold at which the entire lengths of the strips are folded up into a small square. The process is completed by gluing the last flap. See Supplemental Movie 1 for a demonstration [19].

^{*}rp0035vf@ed.ritsumei.ac.jp

[†]hwada@fc.ritsumei.ac.jp

origami tubes [22]. This also leads to an unusually large stretch-twist coupling that may find a potential application in the mechanisms of mode conversions.

We first fabricate a physical model of a paper spring with very compliant hinges, using thin plastic sheets. By measuring the tensile force and twisting, we experimentally quantify its kinematics and mechanics during the actuation, which are corroborated with our finite-element numerical simulations. We then develop a simple analytical theory to understand the massive geometric coupling between rotation and translation, as well as the spring's linear response (Hooke's law) to explain our experimental and numerical data. We further provide an empirical scaling relationship for the force versus extension behavior that may be applicable to high-force regimes where the response is nonlinear. Finally, we measure 3D shape changes of selected plates to gain information on the surface curvature distributions. Visualization of the Gaussian curvatures suggests that a highly stretched region emerges and is localized close to vertices, which may be responsible for the stress-stiffening behavior.

II. STRUCTURE

Before the mechanical test, we characterize the geometry of our paper spring in this section. A unit cell consists of two identical modules, each of which comprises two identical square plates of length a and thickness t ($\ll a$) that are connected with freely rotating (floppy) straight crease lines. Repeating the unit cell defines the periodic structure of our paper spring. (See Supplemental Movie 2 for a 360° view of a spring model [19].) Hereafter, we denote its period as N , for which each strip consists of $2N$ plates [Fig. 2(a)]. Overall, the spring has a discrete helical structure, like many other common springs. See the dashed line in Fig. 2(b). An individual plate has four sides: two are the crease lines (a valley and a mountain crease) and the other two are free. However, in the interfolded configuration, one of the two free sides is always occupied by the crease line of the pairing strip. Thus, in the assembled geometry, only one side of any plate is really force- and moment-free. We denote the other three as the hinge sides. These hinges are all one-dimensionally connected, and each constitutes a single helical frame with a period equal to that of the unit cell; see the white links in Fig. 3 that schematically show our structure. In contrast, the free sides also form a helical structure, but it makes one full helical turn every *four* unit cells with the handedness *opposite* to that of the hinge helix (see the yellow links in Fig. 3). Thus, by definition, there are three such identical helices of the free sides, each of which is separated by the distance of the unit cell along the long axis of the spring. (Note that only one of the three is displayed in Fig. 3.) Therefore, the skeleton of our paper spring may appear as the quadruple-stranded helix: one strand is a short pitch helix of the hinge lines with one handedness, and the other three are long-pitch helices with the opposite handedness.

Note, however, that the exact fourfold rotational symmetry with a regular spiral progression along the long axis is geometrically impossible; the design satisfies the discrete fourfold rotational symmetry only approximately. Our spring actually cannot be represented as a mechanism of rigid

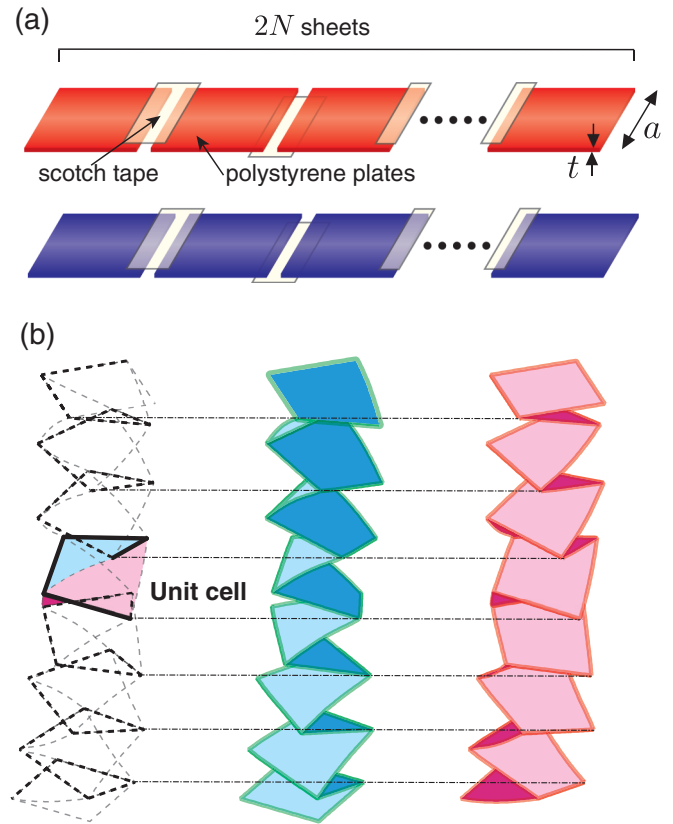


FIG. 2. (a) Schematics of a realization with thin plastic plates of a paper strip folded into a concertina. A floppy crease line is realized with a thin Scotch tape. The two such corrugated strips are assembled into a linear interlocking structure according to the “paper-spring” procedure. (b) Architecture of our paper spring. A pair of accordion-like corrugated strips (blue and red) are interfolded. The highlighted section in the leftmost figure defines a unit cell.

straight lines of constant length linked by the hinges. At any extension, the crease lines must bend, and corresponding plates must also bend and stretch. This is distinctly different from the majority of recent work in which geometrically compatible origami patterns such as Miura-ori were considered [23].

III. EXPERIMENTAL METHOD

To quantify the geometric mechanics of a paper spring, we manually fabricate its experimental model that may be suitable for repeatable measurements. We used commercial polystyrene sheets instead of paper to minimize the effects of anelastic deformations and humidity. An accordion-like strip comprises identical square plates of length a that were cut out from a B4 size plastic sheet with a cutting machine (Silhouette Cameo, Graphtec). Models of various combinations of the geometric parameters (the plate size $a = 20$ and 40 mm, thickness $t = 0.2$ and 0.4 mm, and the periodicity $N = 2.5$ and 6) were fabricated. We have independently determined the Young's modulus of a plastic sheet by measuring a sheet deflection by its own weight and fitting the shape with the theory of Euler elastica under gravity, which yielded $E = 2.5$ – 4.3 GPa.

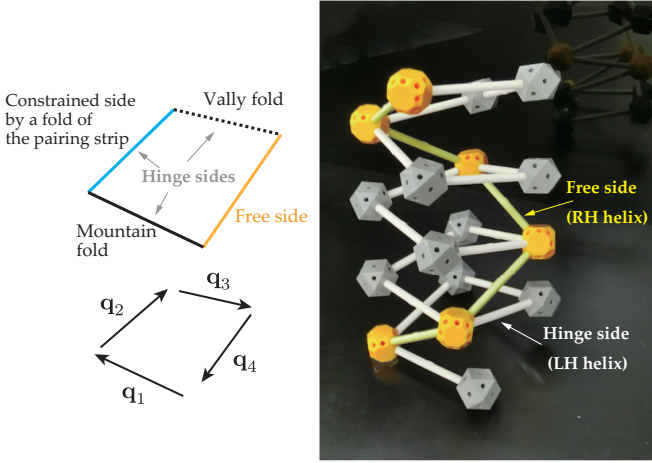


FIG. 3. A schematic physical model representation of the helical structure of the linkages. The white links represent the hinge sides of thin plates, whereas the yellow links represent the free sides. They define the helical skeletons with opposite handedness to each other.

We joined two flat plates with a sufficiently thin Scotch tape that adds a negligible bending stiffness to the resulting crease line [Fig. 2(a)]. This acts as a very compliant hinge that requires almost no force to open the connecting panels. To prevent the taped-together regions from being damaged, the maximum fractional extension of a spring was less than 65% in our experiments.

To construct an entire spring, we start by gluing the terminal plates of the two strips, making them a right angle (Fig. 1). Depending on the order of folding, we can generate a right- or left-handed spring. We complete the construction by again gluing the final surfaces. Note that the energy-minimizing configuration of our spring is the maximally folded one, which differs from usual origami-type springs with finite hinge opening angle and elasticity. Note also that no extension is allowed if the structure comprises perfectly rigid surfaces. Deflections of the plates are thus essential for global deformations of our spring. While stretching, we did not observe any appreciable sliding of the pairing strips, probably due to sufficiently strong static friction forces enhanced by their interlocking structures.

Similarly to a usual elastic spring, our spring twists as it extends. To realize a torque-free measurement, we assembled a left- and right-handed spring that are structurally identical except for the handedness. Stretching of this tandem array allows us to quantify the twist in each spring by measuring the rotation angle Φ at the middle as a function of the end-to-end distance, under the zero net torque condition (Fig. 4). In the stretching test, the whole object is horizontally mounted with one end being fixed in position. In this configuration, the spring was observed to sag weakly under its own weight. The other end is displaced slowly with a stepping motor at a constant speed, and the resulting tensile force is measured by a load cell. We tried several different speeds to confirm that the experiments are performed in quasi-equilibrium condition for which the dependence of the stretching speed is absent. The corresponding deformations are recorded with a digital camera. In selected cases, we also capture the 3D profile of individual panels during stretching in a home-built triangulation

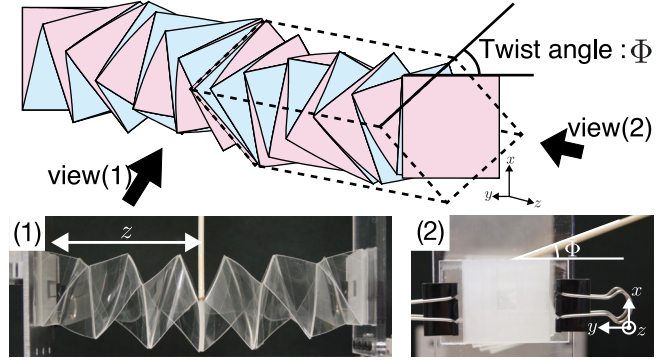


FIG. 4. Definition of the xyz coordinate system, the extension z , and the twist angle Φ in our experiments. The side views [views (1) and (2)] of a real spring model are also shown.

system. The data are then used to calculate the local curvatures to characterize its stretching and bending in the panel.

In all the force versus extension curves shown in the following, the zero displacement point is determined from the dynamic force response. We start by compressing our spring slightly beyond its naturally folded configuration, for which $F = -\infty$. As soon as the compression is relaxed, the force rapidly approaches zero, then increases more slowly as it is further extended. The point where dF/dz changes steeply is identified as the zero displacement point of the spring.

To complement our experimental results, we also conducted finite-element numerical simulations using the commercial package Abaqus (Dassault Systems). A spring is constructed by connecting identical thin elastic plates of thickness $t/a = 0.005\text{--}0.02$ with freely rotating straight line hinges. In the simulations, stretching of an entire structure is investigated in the force-controlled condition. To be more precise, one end of the spring is fixed, say, within the x - y plane, while the other end is pulled by the external force along the z direction that is applied uniformly on the final plate. The equilibrium configuration was obtained by minimizing the elastic energy of a linear isotropic solid by using four-node, quadrilateral shell elements with geometric nonlinearity, Young's modulus $E = 1$ GPa, and Poisson's ratio $\nu = 0.3$ (valid for typical plastic plates that usually have Poisson's ratio $\nu = 0.3\text{--}0.4$). We tested systematically different sets of the mesh sizes and types and confirmed that the results shown in the following are essentially insensitive to those parameters.

IV. RESULTS

In Fig. 5 the measured twisting angle Φ at the middle of the structure is plotted as a function of the rescaled extension $z/(aN)$ for springs of various geometries. Note that the spring length at its full extension is $2aN$, but we rescale z by aN throughout this paper because the extension of our springs never exceed 65% (see Sec. II). Selected experimental snapshots of the tandem springs for period $2N = 12$, size $a = 40$ mm, and thickness $t = 0.4$ mm are shown in the inset of Fig. 5, which compare well with those obtained from our numerical simulations shown in Fig. 6. The scaling plot in Fig. 5 shows that all the experimental and numerical data

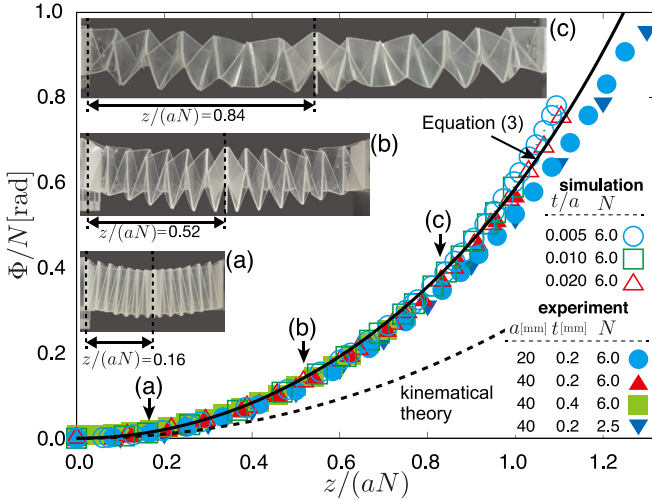


FIG. 5. Twist angle per unit cell, Φ/N , measured as a function of the rescaled extension $z/(aN)$, for springs with different geometries (the sheet size a , the sheet thickness t , and the number of unit cells N). The experimental and numerical data are shown together. The dashed line shows our prediction based on the kinematic theory, while the solid line shows the analytical curve from Eq. (3) with the adjustable parameter $\kappa = 0.73$. Experimental snapshots of the physical spring model for $a = 40$ mm, $t = 0.4$ mm, and $N = 6$ for increasing extension are given in the inset.

collapse onto a single curve, suggesting that the stretch-twist coupling is insensitive to the plate thickness t .

Although an actual deformation involves complex bending and stretching of the plates, the observed twisting behavior of the spring may be predominantly geometric; it can be understood with a purely kinematic consideration. We focus on the helical linkage illustrated in Fig. 3 and assign a set of vectors of constant length a to those association lines. The

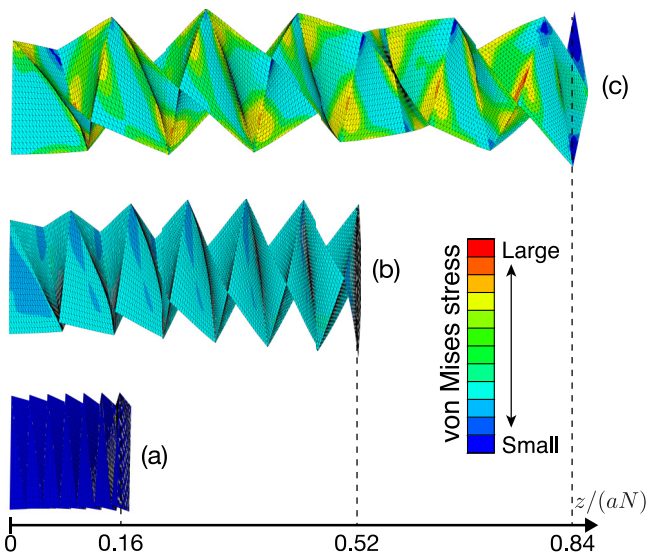


FIG. 6. Configurations of the simulated paper spring of $t/a = 0.02$ and $N = 6$ at different extensions indicated in panels (a)–(c). The color map represents the magnitude of principle (von Mises) stresses.

unit cell, i.e., a full helical turn, is thus composed of a series of four vectors \mathbf{q}_1 – \mathbf{q}_4 (see Fig. 3). To proceed, we make the following simplifying assumptions. First, upon deformation, each association line remains a straight line of fixed length a , making a constant angle $\pi/2 - \theta$ with respect to the stretching axis (z axis):

$$\mathbf{q}_i \cdot \hat{\mathbf{z}} = \sin \theta. \quad (1)$$

Second, any pair of consecutive vectors make a right angle, that is, the plates keep their square vertices upon deformations, which requires

$$\mathbf{q}_i \cdot \mathbf{q}_{i+1} = 0. \quad (2)$$

As discussed in the previous section, these two simplifying assumptions are actually not geometrically compatible but are still useful to derive an effective kinematic theory as long as the sheet deflections remain small enough. We then parametrize the hinge vector as $\mathbf{q}_i = a(\cos \phi_i \cos \theta, \sin \phi_i \cos \theta, \sin \theta)$ and plug them into Eqs. (1) and (2) to obtain $\phi_{i+1} - \phi_i = \cos^{-1}(-\tan^2 \theta)$. The rotational angle of \mathbf{q}_i in the xy plane per single helical turn is $\phi_{i+4} - \phi_i$, which equals 2π for a twistless spring. The net twisting angle per period is thus $\phi_{i+4} - \phi_i - 2\pi = 4(\phi_{i+1} - \phi_i) - 2\pi$, which, for a N -pitch spring, amounts to the total twisting angle $\Phi = 4N \sin^{-1}(\tan^2 \theta)$. On the other hand, the extension per spring is $z = 4aN \sin \theta$. Eliminating θ from these two equations leads to the twist-stretch kinematic relation given by $\Phi(z) = 4N \sin^{-1}\{z^2/[(4aN)^2 - z^2]\}$. In Fig. 5 we compare this prediction with our experimental and numerical data; The theoretical model (the dashed line) does capture the qualitative trend of the data, but there is also some expected quantitative disagreement due to the neglect of elasticity, as noted above. For the configurations of the linkages assumed above, the sheets would have to be considerably stretched, which is kinematically possible, but is actually restrained owing to the sheet elasticity. Thus, the spring undergoes more complex deformations to minimize stretch in the sheets, for which different unit cells may deform differently. As a consequence, the unit cell, on average, may have to twist more than required in the above kinematic theory. This may suggest the need for replacing the plate size a with an effective (smaller) size κa in Eq. (3), where $0 < \kappa < 1$ is an adjustable parameter, for obtaining an improved quantitative agreement in Fig. 5. We thus propose

$$\Phi(z) = 4N \sin^{-1} \left[\frac{z^2}{(4aN)^2 \kappa^2 - z^2} \right]. \quad (3)$$

In Fig. 5 we compare Eq. (3) with our experimental and numerical data, and find good agreement between them, for $\kappa = 0.73$. In the regime studied here, we see $z/4aN \ll 1$, for which we obtain from Eq. (3) $\Phi \approx z^2/(4N\kappa^2 a^2)$. This simple result provides a fairly good approximation over the entire region of the extension z investigated here and should be useful to characterize the twist-stretching coupling of the spring.

In Fig. 7 we show the elastic responses of our spring. The smooth monotonic increase of the stretching force F in Fig. 7(c) confirms the absence of multistability in our spring; it deploys continuously as it is stretched, unlike the other

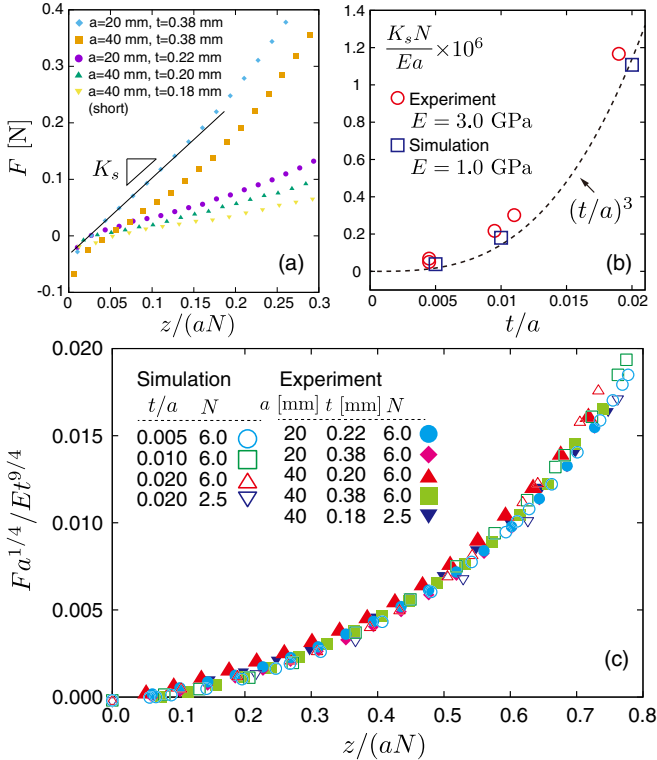


FIG. 7. Measured force F versus extension z curves for springs of various geometries indicated. (a) Linear F - z relation at small extension regime. (b) Spring constant K_s as a function of the thickness t , extracted from the data shown in panel (a). (c) Force vs extension curves in the rescaled form suggested in Eq. (5). The experimental and numerical data are shown together. In rescaling the experimental data, we have used Young's modulus $E = 3.0$ GPa (from the measured range 2.5–4.3 GPa) in order to obtain the best collapse of the data. For the sake of consistency, this value, $E = 3.0$ GPa, is assumed in panel (b).

origami-based structures that can display highly complicated mechanical responses [24–26]. We also confirm that our spring does not show any hysteric force responses during extension and compression.

For small displacement regime, the restoring force of our spring mainly arises from the bending elasticity of the plates. Assuming a uniform deformation for all the plates, the spring extension is $z \sim 2Nu$, where u is the out-of-plane deflection of each plate. The bending curvature of the plate is, thus, $\kappa \sim u/a^2$, for which the bending energy may be given by $E_{\text{bend}} \sim B\kappa^2 a^2 \times 2N \sim 2NBu^2/a^2$, where $B = Et^3/[12(1 - \nu^2)]$ is the bending stiffness. The tensile force F is, thus, found from $F = \partial E_{\text{bend}}/\partial z$, from which we obtain the linear load-displacement relation $F = K_s z$, where the spring constant is given by

$$K_s = (\text{const}) \times \frac{Et^3}{(1 - \nu^2)a^2 N}. \quad (4)$$

In Fig. 7(a) we show the load-displacement curves obtained for a different set of parameters. We determine the experimental spring constant K_s as the initial slope of those load-displacement curves. The same procedure is applied to the simulation data. The resulting K_s from both the experiments

and simulations are then plotted against t/a in Fig. 7(b), which is in good agreement with the theoretical prediction in Eq. (4), i.e., $NK_s/Ea \sim (t/a)^3/(1 - \nu^2)$. Note that some experimental data in Fig. 7(a) do not appear to cross the origin, probably because of imperfections that are unavoidable within the manually prototyped structures, as well as deflections due to gravity. Nevertheless, Fig. 7(a) unambiguously shows the t^3 dependence of the effective spring constant K_s , i.e., the characteristics of the bending elasticity of thin plates. While gravity may have some effect on the prefactor in Eq. (4), we confirm that the linear response of the spring comes predominantly from the pure bending of the faces.

At larger extension, the curve significantly departs from the linear relation owing to geometry-induced stiffening [Fig. 7(c)]. At this finite extension regime, the deformations of the plates involve not only bending but also stretching (twisting), and $F \sim Et^3$ scaling is no longer valid. Considering that a force to stretch a thin sheet scales as $\sim t$, the t dependence of the measured force should range between t and t^3 and may be close to t^3 because the bending is still the dominant mode. We propose the following empirical scaling relationship:

$$F = \frac{Et^{3-\gamma}}{a^{1-\gamma}} f\left(\frac{z}{aN}\right), \quad (5)$$

where $f(x)$ is an as-yet unspecified scaling function characterizing the force curve in Fig. 7(c). We choose the exponent γ in Eq. (5) so that we obtain the best collapse of different sets of data [Fig. 7(c)]. The fitting implies $\gamma = 3/4$, which leads to the scaling relation $F \sim Et^{9/4}/a^{1/4}$, which is reasonably consistent with the mechanics of thin sheets. While the precise functional form of $f(x)$ is unknown, it steeply increases as the extension x increases, indicating the stiffening behavior is due to its interlocking structure. It is an open and intriguing question whether the exponent $\gamma = 3/4$, as well as the scaling function $f(x)$, are universal for paper springs with different folding geometries. In the next section, we further quantify the degree of in-plane stretch in the sheet. For this, we capture 3D deformations of a selected plate at finite spring extension and compare the experimental shape with that from our numerical simulations.

V. 3D SHAPES AND CURVATURES

In Fig. 8(b) we compare an experimentally measured shape of a selected plate at $z/(aN) = 0.625$ with that obtained from the finite-element simulation. For a detail of the experimental method, see the Appendix A. We find excellent agreement, confirming that both methods correctly capture the 3D sheet configurations. Apparently, the plate deflection is dominated by a planar out-of-plane bending [see also Fig. 6(c)]. To examine this in more detail, we derive surface curvatures from the simulated configuration by making use of the discrete differential geometry that yields the mean curvature H and the Gaussian curvature K from the coordinate points of the triangulated midsurfaces [27]. In Figs. 8(c) and 8(d), we show H and K for the spring of extension at $z/(aN) = 0.833$, respectively. Notably, a locally inverted region appears diagonally around the vertices, where H changes its sign from positive to negative, with a strongly negative Gaussian curvature K there, suggesting some vertices are stretched

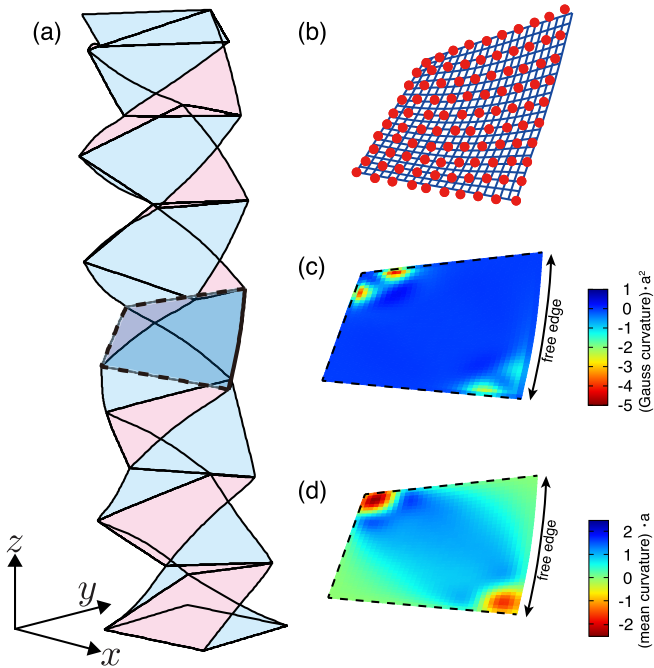


FIG. 8. Thin sheet shape and its surface curvatures. (a) Simulated configuration of a spring for $N = 6$ at extension $z/(aN) = 0.833$. (b) Comparison between the experimental (filled symbols) and numerical (solid lines) shapes of one of the plates in the deforming spring at $z/(aN) = 0.625$ ($a = 40$ mm, $t = 0.4$ mm, and $z = 150$ mm in the experiment). (c) Gaussian curvatures K and (d) mean curvatures H in the plate obtained from the simulation data shown in panel (a). The plate analyzed in panels (c) and (d) is enclosed by the dotted line in panel (a).

substantially. In the rest of the regions where the surface appears cylindrical, K is found to be almost zero, as expected. Thus, we confirm that the deployment of the entire structure does involve the sheet stretching, in agreement with our expectation from Fig. 7(c). A further extension of the whole structure may lead to damage, predominantly, at the taped-together regions. To investigate even higher-force regimes, the current device fabrication may have to be reexamined.

VI. DISCUSSION

In our paper spring geometry, the pairing strips are interlocked; they mutually constrain deformations of the other. This design substantially enhances the structural rigidities because the thin sheets suffer from geometric frustrations and must locally bend and stretch, yet keeping its overall structural flexibility. For a sufficiently small extension regime, our spring is very soft and can bend just like a toy Slinky. Beyond this angle of the small extension, this overconstraining design restricts the system to one dominant mode of deformation to deploy itself—a simple extension and compression along its major axis. As it extends, while the structure can still deflect globally and may behave flexibly, the global bending becomes increasingly stiffer.

A remarkable feature during the actuation is the strong coupling of the global twisting to the stretching mode (see Fig. 5). For the deployment, one end of the structure must

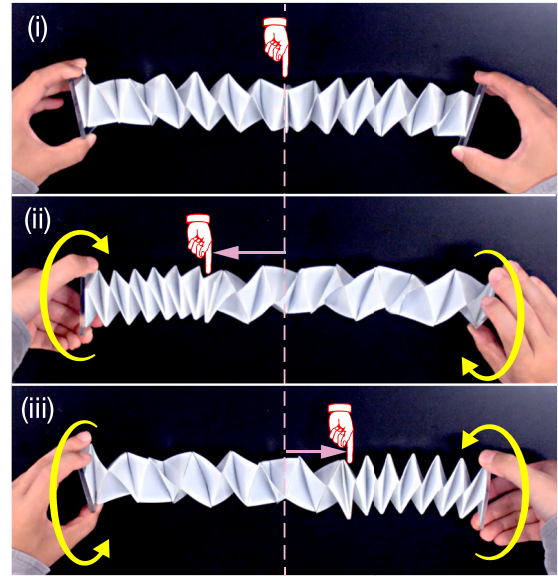


FIG. 9. Demonstration of the direct conversion of the end rotation to the linear translational motion with a tandem assembly of a left- and right-handed spring. This kinematic coupling is reciprocal: force applied at the middle of the structure can induce the rotation of one end of the structure with respect to the other. See also the Supplemental Movie 3 [19].

rotate with respect to the other. Using this tight torque-force reciprocal relation, we envision a direct mechanical transduction of a torque applied at the ends to a linear displacement in a programmable way. For example, in a tandem arrangement of a left- and right-handed spring, torques applied at the ends allow for a linear translation and a precise positioning of the middle part because one spring is extended (compressed) while the other is compressed (extended). (See Supplemental Movie 3 for a demonstration [19].) Furthermore, the range of the distance of the translation can be tuned accurately with the applied load at the ends. This metamaterial-like property is robust in our paper spring architecture and will be favorable for potential applications in the design of a range of mechanical devices including soft robotics.

Note that the geometric twist-stretch coupling is a general feature for chiral slender structures, from nano- to macroscales [28,29]. For example, a twisted origami bellows also shows untwisting (twisting) behavior during extension (compression). By connecting left- and right-handed such bellows (Fig. 10), we observe a similar behavior to our paper spring as shown in Fig. 9. (See Supplemental Movie 4 for a demonstration [19].) However, because of its multistable nature, the extension and compression behavior of the tandem origami bellows is not really smooth. The faces are bistable and can often snap locally when the bellows is stretched sufficiently. This induces a locally stable natural curvature, making the whole structure helical as shown in Fig. 10. In contrast, our spring paper model is robustly monostable, smoothly expanding and shrinking as it twists and untwists. Its kinematics is precisely described by Eq. (3), which is fully predictable, reproducible, and controllable. In addition, the coupling here is distinctly prominent compared with many other slender chiral structures. Regarding the fabrication

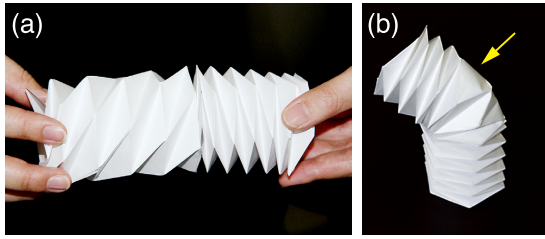


FIG. 10. (a) Demonstration of the direct conversion of the end rotation to the linear translational motion with a tandem assembly of a left- and right-handed twisted origami bellows. (b) Origami bellows with a defect (a locally inverted face) after the deployment.

aspects, the crease pattern of our paper spring is much simpler than those of typical origami bellows and might be suitable for envisioning automatic productions in the future. These advantages may make our paper spring a unique system as a reversible torque-force conversion device.

VII. CONCLUSION

In this paper, by combining fabrication, experiments, numerical simulations, and analytical theory, we have investigated the geometrical and mechanical properties of a paper spring: an origami-based structure made by folding and gluing together two thin strips of paper. To the best of the authors' knowledge, this is the first attempt to characterize the nonlinear mechanics of this popular origami-like motif. In fact, a paper spring is very easy to make, much easier than more typical origami patterns. (Try it yourself.) From this simplest possible crease pattern, a rich mechanical and structural behavior is shown to emerge. Through systematic experiments, we have revealed the strong geometric coupling between stretch and twist, as well as the increasing stiffness

against a global bending during unfolding. This deployment kinematics could provide a unique avenue of the mode conversion for potential applications in mechanical designs. We have also addressed the origin of its springy response, quantifying the bending and stretching in the sheet panel by capturing its shape and surface curvatures. Our present study will serve as the important first step for the physical understanding of this unique deployable structure. At this stage, a number of aspects are still open to further detailed experimental and numerical investigations.

ACKNOWLEDGMENTS

We thank K. Suehiro, T. G. Sano, and Y. Murayama for helpful discussions. Financial support from JSPS KAKENHI (Grants No. 18K13519 and No. 18K18741) (to H.W.) and the Sasakawa Scientific Research Grant from The Japan Science Society and Grant-in-Aid for JSPS Research Fellow (DC1, No. 19J22381) (to T.Y.) is acknowledged.

APPENDIX: 3D SHAPE MEASUREMENTS

For the stereoscopic reconstruction, we first placed 100 black mill-metric dots on one of the faces of a spring, regularly placed on a square grid with a grid size of about 4 mm. The spring was stretched to a given extension and was positioned about 1.5 m from a digital camera. Images were taken at two different viewpoints from 300 mm away, with their optical axes set in parallel. The coordinates of the dots in the picture plane were obtained by processing the photographs using ImageJ software. We then reconstructed the corresponding 3D coordinates in real space by applying a scheme similar to a standard triangulation method. We tested our method with centimeter-sized objects of known shapes, such as a cube and a sphere, and confirmed its accuracy within 2.3% error.

-
- [1] E. D. Demaine, M. L. Demaine, D. Koschitz, and T. Tachi, in *Proceedings of the 35th Annual Symposium of IABSE/52nd Annual Symposium of IASS/6th International Conference on Space Structures, London, Sept. 20–23, 2011* (IABSE/IASS, Zurich, Switzerland, 2011), Paper No. 10065184, p. 593.
 - [2] T. Tachi, *J. Mech. Des.* **135**, 111006 (2013).
 - [3] A. Lebé, *Int. J. Space Struct.* **30**, 55 (2015).
 - [4] H. Kobayashi, B. Kresling, and J. F. V. Vincent, *Proc. R. Soc. B* **265**, 147 (1998).
 - [5] M. J. Harrington, K. Razghandi, F. Ditsch, L. Guiducci, M. Rueggeberg, J. W. C. Dunlop, P. Fratzi, C. Neinhuis, and I. Burgert, *Nat. Commun.* **2**, 337 (2011).
 - [6] W. T. M. Forbes, *J. NY Entomol. Soc.* **34**, 91 (1926).
 - [7] K. Saito, S. Nomura, S. Yamamoto, R. Niyama, and Y. Okabe, *Proc. Natl. Acad. Sci. USA* **114**, 5624 (2017).
 - [8] K. Miura, *Inst. Space Astronaut. Sci. Rep.* **618**, 1 (1985).
 - [9] J. T. Bruton, T. G. Nelson, T. K. Zimmerman, J. D. Fernelius, S. P. Magleby, and L. L. Howell, *R. Soc. Open Sci.* **3**, 160429 (2016).
 - [10] K. Kuribayashi, K. Tsuchiya, Z. You, D. Tomus, M. Umemoto, and M. Sasaki, *Mater. Sci. Eng. A* **419**, 131 (2005).
 - [11] K. Bertoldi, V. Vitelli, J. Christensen, and M. van Hecke, *Nat. Rev. Mater.* **2**, 17066 (2017).
 - [12] T. Hull, *Project Origami* (CRC Press, Boca Raton, FL, 2013).
 - [13] Z. Y. Wei, Z. V. Guo, L. Dudte, H. Y. Liang, and L. Mahadevan, *Phys. Rev. Lett.* **110**, 215501 (2013).
 - [14] J. L. Silverberg, A. A. Evans, L. McLeod, R. C. Hayward, T. Hull, C. D. Santangelo, and I. Cohen, *Science* **345**, 647 (2014).
 - [15] J. L. Silverberg, J.-H. Ha, A. A. Evans, B. Liu, T. Hull, C. D. Santangelo, R. J. Lang, R. C. Hayward, and I. Cohen, *Nat. Mater.* **14**, 389 (2015).
 - [16] F. Lechenault and M. Adda-Bedia, *Phys. Rev. Lett.* **115**, 235501 (2015).
 - [17] J. A. Faber, A. F. Arrieta, and A. R. Studart, *Science* **359**, 1386 (2018).
 - [18] C. R. Calladine, *Theory of Shell Structure* (Cambridge University Press, Cambridge, 1983).
 - [19] See Supplemental Material at <http://link.aps.org/supplemental/10.1103/PhysRevE.100.013003> for the movies 1-4 that show experimental demonstrations for the fabrication, structure, and kinematics of paper springs and origami bellows.

- [20] There are many other types of paper springs, including the one created by Jeff Beynon that can be made from a single piece of paper without cutting or gluing [30].
- [21] F. Lechenault, B. Thiria, and M. Adda-Bedia, *Phys. Rev. Lett.* **112**, 244301 (2014).
- [22] E. T. Filipov, T. Tachi, and G. H. Paulino, *Proc. Natl. Acad. Sci. USA* **112**, 12321 (2015).
- [23] M. Schenk and S. D. Guest, *Proc. Natl. Acad. Sci. USA* **110**, 3276 (2013).
- [24] T. Tachi and K. Miura, *J. Int. Assoc. Shell Spat. Struct.* **53**, 217 (2012).
- [25] H. Yasuda and J. Yang, *Phys. Rev. Lett.* **114**, 185502 (2015).
- [26] A. Reid, F. Lechenault, S. Rica, and M. Adda-Bedia, *Phys. Rev. E* **95**, 013002 (2017).
- [27] M. Meyer, M. Desbrun, P. Schröder, and A. H. Barr, in *Visualization and Mathematics III. Mathematics and Visualization*, edited by H. C. Hege and K. Polthier (Springer, Berlin, 2003), pp. 35–57.
- [28] R. D. Kamien, T. C. Lubensky, P. Nelson, and C. S. O’Hern, *Europhys. Lett.* **38**, 237 (1997).
- [29] T. Frenzel, M. Kadie, and M. Wegener, *Science* **358**, 1072 (2017).
- [30] C. C. Min and H. Suzuki, in *Manufacturing Systems and Technologies for the New Frontier* (Springer, London, 2008), pp. 159–162.